PTEP

Prog. Theor. Exp. Phys. **2023** 043B04(17 pages)
DOI: 10.1093/ptep/ptad045

IYBSSD2022
International Year
of Basic Sciences
for Sustainable Development

# String is a double slit

Koji Hashimoto[1,*], Yoshinori Matsuo[2], and Takuya Yoda[1]

[1]*Department of Physics, Kyoto University, Sakyo-ku, Kyoto 606-8502, Japan*
[2]*Department of Physics, Kindai University, Higashi-Osaka, Osaka 577-8502, Japan*
*E-mail: koji@scphys.kyoto-u.ac.jp

Received March 3, 2023; Accepted March 30, 2023; Published March 31, 2023

We perform imaging of a fundamental string from string scattering amplitudes, and show that its image is a double slit.

Subject Index B20, B24, B29, B87

## 1. Introduction and summary

Have you ever seen a string? Since the discovery of string theory as a candidate for the unifying theory, the rich dynamics of strings has been revealed. For example, strings can be reconnected and be torn apart. They can be attached to branes or absorbed into. Furthermore, strings can undergo the transition to black holes. The black hole–string correspondence [1,2] (see also [3,4]) tells us that a single long string tends to shrink, if its self-gravity is turned on, and finally it becomes a black hole when its typical size reaches the Schwarzschild radius. Although it is expected that strings answer the microscopic degrees of freedom of black holes, secrets are still hidden inside horizons.

If possible, it would be worthwhile to shoot photos of a string. In physics and engineering, imaging technologies are widely used to take pictures of various objects. Imaging technologies allow us to investigate the inner structures of objects when they are hidden from the outside. Even if their structures are highly complicated, imaging technologies provide us clear and intuitive ways to understand the structures. For example, the structure of the human body is highly complicated and cannot be seen directly from the outside. However, various imaging technologies, such as X-ray imaging and ultrasound wave imaging, enable us to study the functions of human organs, and find the causes of disease.

The string is a suitable target for applying such imaging technologies. The inner structure of a long string is unclear and expected to be highly complicated. And in fact, the traditional perturbative string theory is defined only through string scattering amplitudes, and thus if one wants to see a fundamental string itself, one needs the imaging from the scattering amplitudes, solving the inverse problem—it is a reconstruction of the internal structure by the scattering wave data.


Funded by SCOAP[3]. SCOAP3 and OUP support the goals of the International Year of Basic Sciences for Sustainable Development.

In this paper, as the first step, we study tree-level scattering amplitudes of open bosonic fundamental strings, and reconstruct their images from the amplitudes. The imaging is just a Fourier transformation, as the standard optical theory tells. The reconstruction method works as an eye to look inside the scattering processes. The results of the imaging show that the images of the fundamental string are double slits.

String scattering amplitudes have a lot of zeros, and we find that their pattern of brightness/darkness observed at the spatial infinity matches that of the standard double-slit experiment. This is the reason why the imaging via the string scattering amplitudes results in images of double slits.

As the simplest example, we consider the scattering of tachyons. We apply the imaging method to the $s$-channel pole of the Veneziano amplitude, and find that the image is a double slit. In the large-level limit of the pole mass, the coincidence with the double slit is exact. We also apply the imaging method to the $s$-channel pole of the string decay amplitude of a highly excited string (HES), using the amplitude obtained in [5,6]. We find that the image is a set of multiple slits aligned on a straight line.

Slits in the images of the string scattering amplitudes are separated by the typical length of the fundamental string at the excited $s$-channel pole, which leads us to interpret that the slits are end points of the string.

Since the imaging technologies are natural to be applied to string theory, more applications in various situations will reveal the hidden structure of a fundamental string. For example, the differences between ordinary quantum field theories and string theory, such as nonlocality, finiteness, and chaos, may be visualized in this imaging process.

This paper is organized as follows. In Sect. 2, we review the standard double-slit experiment, and present an imaging method to reconstruct a double-slit image from the amplitude on a screen. In Sect. 3, we study the Veneziano amplitude, and show that the image of a fundamental string read from the amplitude is indeed a double slit. In Sect. 4, we apply the same method to another scattering process: an HES decaying into two tachyons, and show that its image is a multi-slit. In Sect. 5, we provide a possible interpretation of our results and discuss some implications for string physics.

## 2. Double-slit experiment

In this section, we review the standard double-slit experiment, and a method to reconstruct the image from the amplitude on a screen, to demonstrate that the amplitudes actually encode the image of the double slit.

Let us put two slits $S_1, S_2$ on $(z, x) = (\pm l/2, 0)$, and place the center of a spherical screen of radius $L \gg l$ at the origin. A wave with wavelength $\lambda_{\rm ds}$ passes through the slits from the negative to the positive $x$-direction. An observer P is placed at $(z, x) = (L\cos\theta', L\sin\theta')$ on the screen. See Fig. 1.

If the screen is sufficiently large, i.e. $L \gg l$, the difference of two optical paths is given by

$$\overline{\mathrm{S_2P}} - \overline{\mathrm{S_1P}} \simeq l\cos\theta'. \tag{1}$$

Thus the condition that the amplitude at P vanishes is

$$\cos\theta' \simeq \frac{k'}{2}\frac{\lambda_{\rm ds}}{l} \tag{2}$$

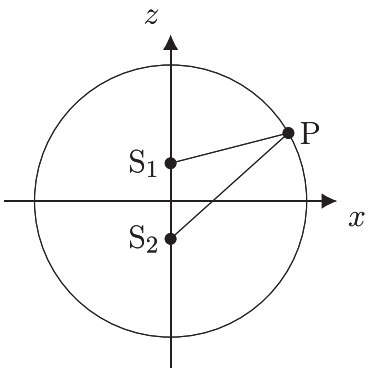


**Fig. 1.** Double slit is put at $S_1$ and $S_2$, and scattered wave is observed at point P.

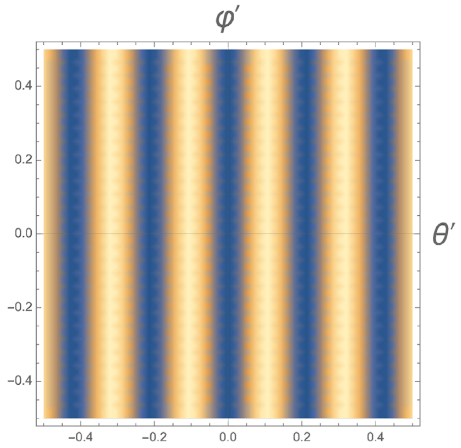


**Fig. 2.** The amplitude of waves in the double-slit experiment, for $\pi l/\lambda_{ds} = 15$.

where $k'$ is an odd integer. More precisely, supposing that a spherical wave is emitted from the two slits with identical phase and amplitude $A$, the wave amplitude on the sphere placed at the spatial infinity $L(\gg l)$ is

$$\mathcal{A}(\theta', \varphi') \simeq 2A \cos\left(\frac{\pi l}{\lambda_{ds}} \cos\theta'\right). \tag{3}$$

Zeros of this amplitude are given by Eq. (2). The result is independent of another spherical coordinate $\varphi'$ as the slits are separated along the $z$-axis in this case.

The wave amplitude itself does not give the image of the slit, as understood in Fig. 2. Optical wave theory provides a method for the imaging. The popular method is just to put a lens of a finite size $d$ on the celestial sphere, and convert the wave amplitude with the frequency $\omega = 2\pi/\lambda_{ds}$ into the image on a virtual screen located at a focal point of the lens. The formula for converting the amplitude to the image is approximated just by a Fourier transformation for $L \gg l$ (see [7,8] for more details and brief reviews of the formula):

$$I(X, Y) = \frac{1}{(2d)^2 \sin\theta'_0} \int_{\theta'_0-d}^{\theta'_0+d} d\theta' \int_{\varphi'_0-d/\sin\theta'_0}^{\varphi'_0+d/\sin\theta'_0} d\varphi' e^{i\omega((\theta'-\theta'_0)X+(\varphi'-\varphi'_0)Y)} \mathcal{A}(\theta', \varphi'). \tag{4}$$

Here the coordinate $(X, Y)$ is the one on the virtual screen placed behind the lens, so the image $I$ of the optical wave is produced on that $XY$-plane. The location of the center of the lens is at $(\theta', \varphi') = (\theta'_0, \phi'_0)$, and a rectangular shape of the lens region is adopted for computational simplicity.

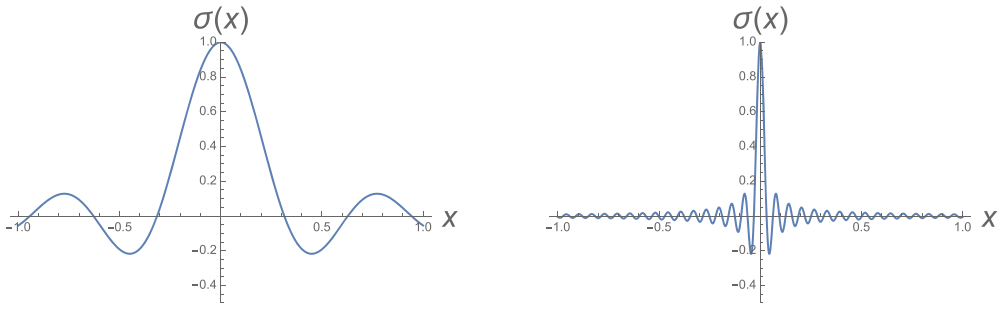


**Fig. 3.** The lens resolution, seen in the behavior of the function $\sigma(x)$ in Eq. (6), for $2\pi d/\lambda_{ds} = 10$ (left) and for $2\pi d/\lambda_{ds} = 100$ (right). For large $d/\lambda_{ds}$ (meaning that the wavelength is small enough that it detects many oscillations of the amplitude), this function is highly peaked at $x = 0$, and the resolution is high.

The lens size $d$ needs to cover at least several zeros of the amplitude to find a sharp image, otherwise the image is blurred and no structure can be reconstructed from the amplitude. In the present case of the double-slit experiment, when one takes the limit $l \gg \lambda_{ds}$ the zeros of the amplitude are aligned densely, so the lens size $d$ can be taken as quite small compared to $2\pi$. It means that the curvature effect of the celestial sphere in the imaging can be ignored and the formula Eq. (4) is validated.

Let us substitute the double-slit amplitude Eq. (3) into the imaging formula Eq. (4) and check if the image reproduces the shape (location) of the slits. The result is

$$I(X, Y) = A(-1)^{\tilde{k}} \sigma\left(Y/\sin\theta_0'\right)\left(\sigma\left(X - \frac{l\sin\theta_0'}{2}\right) + \sigma\left(X + \frac{l\sin\theta_0'}{2}\right)\right) \tag{5}$$

where we have defined

$$\sigma(x) \equiv \frac{\sin\left(\frac{2\pi d}{\lambda_{ds}}x\right)}{\frac{2\pi d}{\lambda_{ds}}x}. \tag{6}$$

See Fig. 3 for the meaning of this function $\sigma(x)$. The calculation is straightforward but we have just assumed that the center of the location of the lens satisfies the condition

$$\frac{l}{\lambda_{ds}}\cos\theta_0' = \tilde{k} \in \mathbf{Z} \tag{7}$$

to simplify the result. It can be met easily because we can find such an integer in the limit $l \gg \lambda_{ds}$ which we took as described above.

The density plots of the image function in Eq. (5) are shown in Fig. 4. One clearly finds the position of the double slits. The parameters are chosen as: $2\pi d/\lambda_{ds} = 30$ and $l = 1$. The left figure is the image of the lens put at $(\theta_0', \varphi_0') = (\pi/2, 0)$. The location $\theta_0' = \pi/2$ means that the lens is put at the right-hand side in Fig. 1, facing the double slits head-on, and the distance between the images of the two slits should be the largest. On the other hand, when the location of the viewer is shifted in the $z$-direction in Fig. 1, the distance between the images of the slits should decrease. In fact, as seen in the middle and the right figures in Fig. 4, for $(\theta_0', \varphi_0') = (\pi/3, 0)$ and for $(\theta_0', \varphi_0') = (\pi/4, 0)$, respectively, one finds a consistent behavior.

In the next section, we apply this method to string scattering amplitudes, and see the images of the fundamental string.

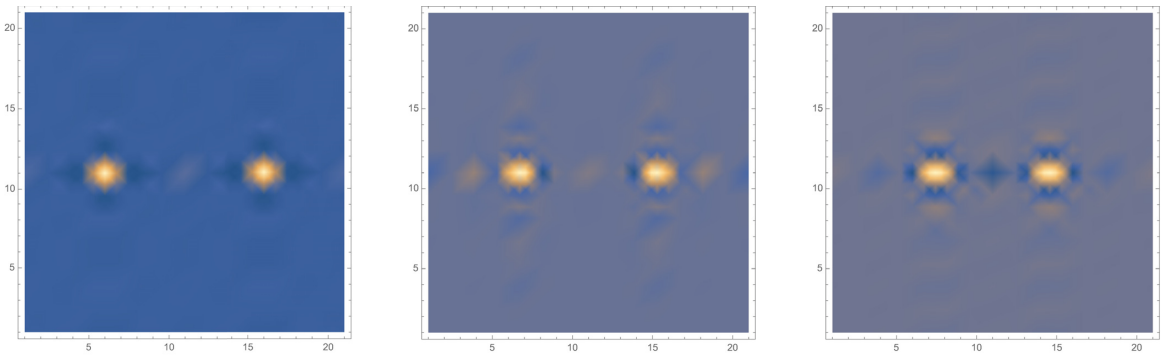

**Fig. 4.** The $X$-$Y$ images of the double-slit experiment, reconstructed from the wave amplitudes at the spatial infinity. Left: seen from the head-on point $(\theta_0', \varphi_0') = (\pi/2, 0)$ facing the aligned slit. Middle: $(\theta_0', \varphi_0') = (\pi/3, 0)$. Right: $(\theta_0', \varphi_0') = (\pi/4, 0)$. As the viewer shifts from the head-on point, the distance between the slits decreases by the function $\sin\theta_0'$ consistently.

## 3. Images of string via Veneziano amplitude

In this section, we obtain the images of a fundamental string by using the Veneziano amplitude, and show that the fundamental string is a double slit.

More specifically, we point out that the zeros of the Veneziano amplitude match the ones of the double-slit amplitude described in Sect. 2. Then we reconstruct images of a string by the Fourier transformation of the Veneziano amplitude. The images show two columns (which are "slits") standing apart at a distance of a typical length of strings.

### 3.1. *Veneziano amplitude and its zeros*

First, we describe our notation of the Veneziano amplitude, tachyon-tachyon to tachyon-tachyon scattering amplitude.

We label its four vertices with 1, 2, 2′, 1′. The momentum conservation law is

$$0 = p_1 + p_2 + p_2' + p_1'. \tag{8}$$

Since each vertex is a tachyon, we have the on-shell condition

$$p_1^2 = p_2^2 = p_2'^2 = p_1'^2 = -(-2). \tag{9}$$

Here, we conventionally chose $\alpha' = 1/2$. In the following computations, we will use the same unit. The Mandelstam variables are defined as

$$s = -(p_1 + p_2)^2 = -\left(p_1' + p_2'\right)^2, \tag{10}$$

$$t = -\left(p_1 + p_2'\right)^2 = -\left(p_1' + p_2\right)^2, \tag{11}$$

$$u = -\left(p_1 + p_1'\right)^2 = -\left(p_2 + p_2'\right)^2. \tag{12}$$

These satisfy an identity

$$s + t + u = 4 \cdot (-2). \tag{13}$$

The Veneziano amplitude [9] is given by

$$\mathcal{A}^{\text{Ven}} = 2\left[\mathcal{A}_{st}^{\text{Ven}} + \mathcal{A}_{tu}^{\text{Ven}} + \mathcal{A}_{us}^{\text{Ven}}\right], \tag{14}$$

where

$$\mathcal{A}_{xy}^{\text{Ven}} = \frac{\Gamma(-\alpha(x))\Gamma(-\alpha(y))}{\Gamma(-\alpha(x) - \alpha(y))}, \quad \alpha(x) = 1 + x/2. \tag{15}$$

The amplitude has $s$-channel poles at $s = 2n$ for integers $n \geq -1$. Since we are interested in the images of a string formed at the scattering, we pull out one of the $s$-channel poles and look at the residue of the pole of the Veneziano amplitude. Using the reflection formula of the Gamma function and the identity in Eq. (13), the residue of the $s$-channel pole is

$$\begin{aligned}\tilde{\mathcal{A}}_s^{\text{Ven}} &= \lim_{s\to 2n} \frac{\sin\pi(-1-s/2)}{\pi}\left(\mathcal{A}_{st}^{\text{Ven}} + \mathcal{A}_{us}^{\text{Ven}}\right) \\ &= \frac{1}{\Gamma(2+n)}\left[\frac{\Gamma(-1-t/2)}{\Gamma(-2-n-t/2)} + (t \leftrightarrow u)\right] = \frac{1}{\Gamma(2+n)}\left[\frac{\Gamma(-1-t/2)}{\Gamma(2+u/2)} + (t \leftrightarrow u)\right].\end{aligned} \tag{16}$$

To evaluate this amplitude, we denote the magnitude of the momentum of the incoming tachyons as $p$. In the center-of-mass frame, the momenta can be generically parametrized as

$$\begin{aligned} p_1 &= \begin{pmatrix} \sqrt{p^2-2} \\ p\sin\theta \\ 0 \\ p\cos\theta \end{pmatrix}, \quad -p_1' = \begin{pmatrix} \sqrt{p^2-2} \\ p\sin\theta'\cos\varphi' \\ p\sin\theta'\sin\varphi' \\ p\cos\theta' \end{pmatrix}, \\ p_2 &= \begin{pmatrix} \sqrt{p^2-2} \\ -p\sin\theta \\ 0 \\ -p\cos\theta \end{pmatrix}, \quad -p_2' = \begin{pmatrix} \sqrt{p^2-2} \\ -p\sin\theta'\cos\varphi' \\ -p\sin\theta'\sin\varphi' \\ -p\cos\theta' \end{pmatrix}. \end{aligned} \tag{17}$$

The parameter $\theta$, which measures the angle of the incoming tachyon against the $z$-axis, will be fixed later for convenience in numerical computations. Under this parametrization, the Mandelstam variables are expressed as

$$s = 4(p^2-2) = 2n, \tag{18}$$

$$t = -2p^2(1+\cos\theta\cos\theta' + \sin\theta\sin\theta'\cos\varphi'), \tag{19}$$

$$u = -2p^2(1-\cos\theta\cos\theta' - \sin\theta\sin\theta'\cos\varphi'). \tag{20}$$

Let us look for zeros of the residue of the $s$-channel pole of the amplitude in Eq. (16). It is zero if and only if

$$\begin{aligned} 0 &= \Gamma(-1-t/2)\Gamma(2+t/2) + (t \leftrightarrow u) \\ &= \frac{\pi}{\sin\pi(-1-t/2)} + (t \leftrightarrow u). \end{aligned} \tag{21}$$

This condition is equivalent to

$$\pi(-1-t/2) + \pi(-1-u/2) = 2\mathbf{Z}\pi, \tag{22}$$

$$\text{or} \quad \pi(-1-t/2) - \pi(-1-u/2) = (2\mathbf{Z}-1)\pi. \tag{23}$$

If $n$ is even, the first equation is satisfied for any angles. Then the amplitude is trivially zero. In the following discussion, we assume that $n$ is odd. The second equation reduces to

$$\cos\theta\cos\theta' + \sin\theta\sin\theta'\cos\varphi' = \frac{2\mathbf{Z}-1}{n+4}. \tag{24}$$

Fixing $\theta = 0$ makes clear a comparison of this result to the double-slit experiment in Sect. 2. In the present case the zeros of the amplitude are at

$$\cos\theta' = \frac{2k+n}{n+4}, \tag{25}$$

for an integer $k \in \mathbf{Z}$. Rewriting this as

$$\cos\theta' \simeq \frac{k'}{n+4} = \frac{k'}{2p^2}, \tag{26}$$

where $k'$ is an odd integer, $k' \in 2\mathbf{Z} - 1$, we find that the location of the zeros is exactly the same as that of the double-slit experiment, Eq. (2), with the replacement

$$p^2 = \frac{l}{\lambda_{\rm ds}}. \tag{27}$$

Here $p$ is the magnitude of the tachyon momentum in the Veneziano amplitude, while $l$ ($\lambda_{\rm ds}$) is the slit-separation (wavelength) in the double-slit experiment.

We have found here that the zeros of the Veneziano amplitude coincide completely with the double-slit experiment. In the next subsection, we look at the Veneziano amplitude in more detail and will find that indeed the imaging of the fundamental string results in a double slit in the $n \to \infty$ limit.

### 3.2. *Imaging of a fundamental string*

Here first we present images of a string by straightforward numerical evaluations, and after that, we analyze the images analytically in a certain limit to extract the structure.

The imaging formula described in Sect. 2 is

$$I(X, Y) = \frac{1}{(2d)^2 \sin\theta'_0} \int_{\theta'_0-d}^{\theta'_0+d} d\theta' \int_{\varphi'_0-d/\sin\theta'_0}^{\varphi'_0+d/\sin\theta'_0} d\varphi' e^{ip((\theta'-\theta'_0)X+(\varphi'-\varphi'_0)Y)} \tilde{\mathcal{A}}_s^{\rm Ven}(\theta', \varphi'). \tag{28}$$

Here $d$ is the size of the lens whose center is put at $(\theta', \varphi') = (\theta'_0, \varphi'_0)$. The lens is applied to the wave signal $\tilde{\mathcal{A}}_s^{\rm Ven}(\theta', \varphi')$ which reached the asymptotic infinity with the angle $(\theta', \varphi')$ in the 2-dimensional spherical coordinate. The frequency of the wave, appearing in the formula Eq. (4), is now given by the tachyon momentum $p$. The wave amplitude is taken as the residue of the $s$-channel pole at $s = 2n$, of the Veneziano amplitude in Eq. (16).

A straightforward numerical evaluation of the imaging in Eq. (28) produces the images shown in Figs. 5 and 6. Since the tachyon scattering is in the center-of-mass frame, we can fix $\theta$ without losing generality. Figures 5 and 6 are for $\theta = \pi/2$ and $\theta = \pi/4$, respectively, with $n = 11$. We find that in fact the images of the fundamental string are those of the double slits.

Analytic estimation of the image, which is useful to study the structure of the images, is possible. Let us investigate in particular the separation between the two slits. For simplicity let us take $\theta = 0$ to eliminate the $\varphi'$-dependence of the amplitude in Eq. (16). We find

$$\tilde{\mathcal{A}}_s^{\rm Ven} = \frac{1}{(n+1)!} \left[ \frac{\Gamma\left(\frac{n}{2} + 1 - \frac{n+4}{2}\cos\theta'\right)}{\Gamma\left(-\frac{n}{2} - \frac{n+4}{2}\cos\theta'\right)} + \frac{\Gamma\left(\frac{n}{2} + 1 + \frac{n+4}{2}\cos\theta'\right)}{\Gamma\left(-\frac{n}{2} + \frac{n+4}{2}\cos\theta'\right)} \right]. \tag{29}$$

To perform an analytic evaluation of the imaging formula for this amplitude, we need to find a simplified expression of the amplitude. A simplification occurs when we take a large $n$. Indeed, in the large $n$ limit the zeros are very close to each other, thus a small lens is sufficient for the imaging. This means that we need only a local expression of Eq. (29) around a certain value of $\theta'$.

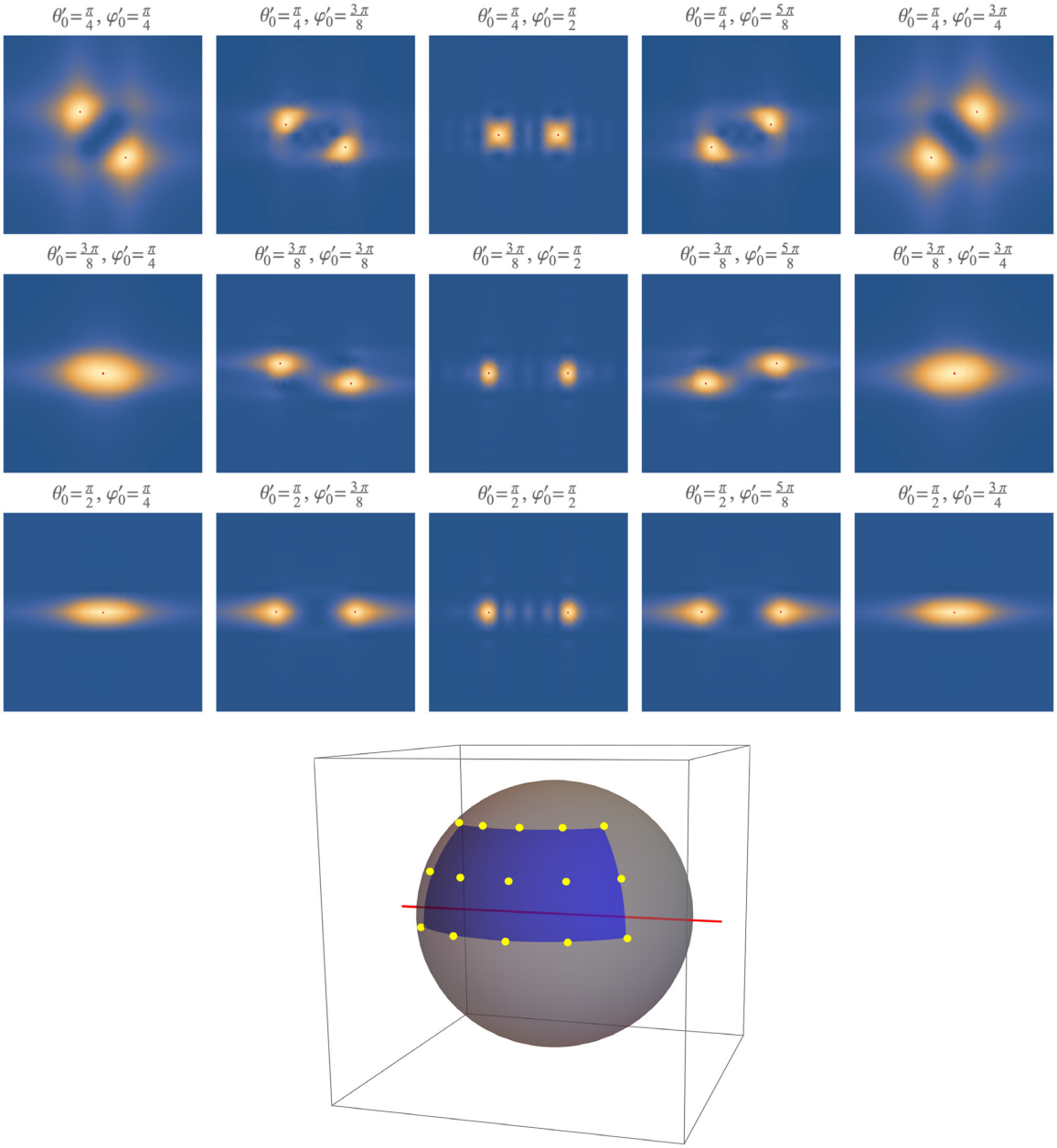


**Fig. 5.** (Top) Images of a fundamental string, extracted and reconstructed from the $s$-channel pole of the Veneziano amplitude. The incoming angle is chosen as $\theta = \pi/2$. Various figures are for different choices of the viewer's location (lens location) specified by $(\theta'_0, \varphi'_0)$. Brightness of these density plots is normalized in each plot. The red points in the images are the brightest points. (Bottom) The incoming trajectory (red line) and the observed points on the celestial sphere (yellow circles).

Below, we obtain a simplified local expression of the amplitude around a zero specified by the integer $k$ given in Eq. (24). We present two expressions: one is for the region around the zero with $k = -(n+1)/2$, which means the expression for $\theta' \sim 0$ in the large $n$ limit; and the other is for a generic value of $k$.

First, notice that the amplitude in Eq. (29) can be locally approximated by

$$\tilde{\mathcal{A}}_s^{\text{Ven}} \sim f(\theta') \cos\left(c\theta'\right), \tag{30}$$

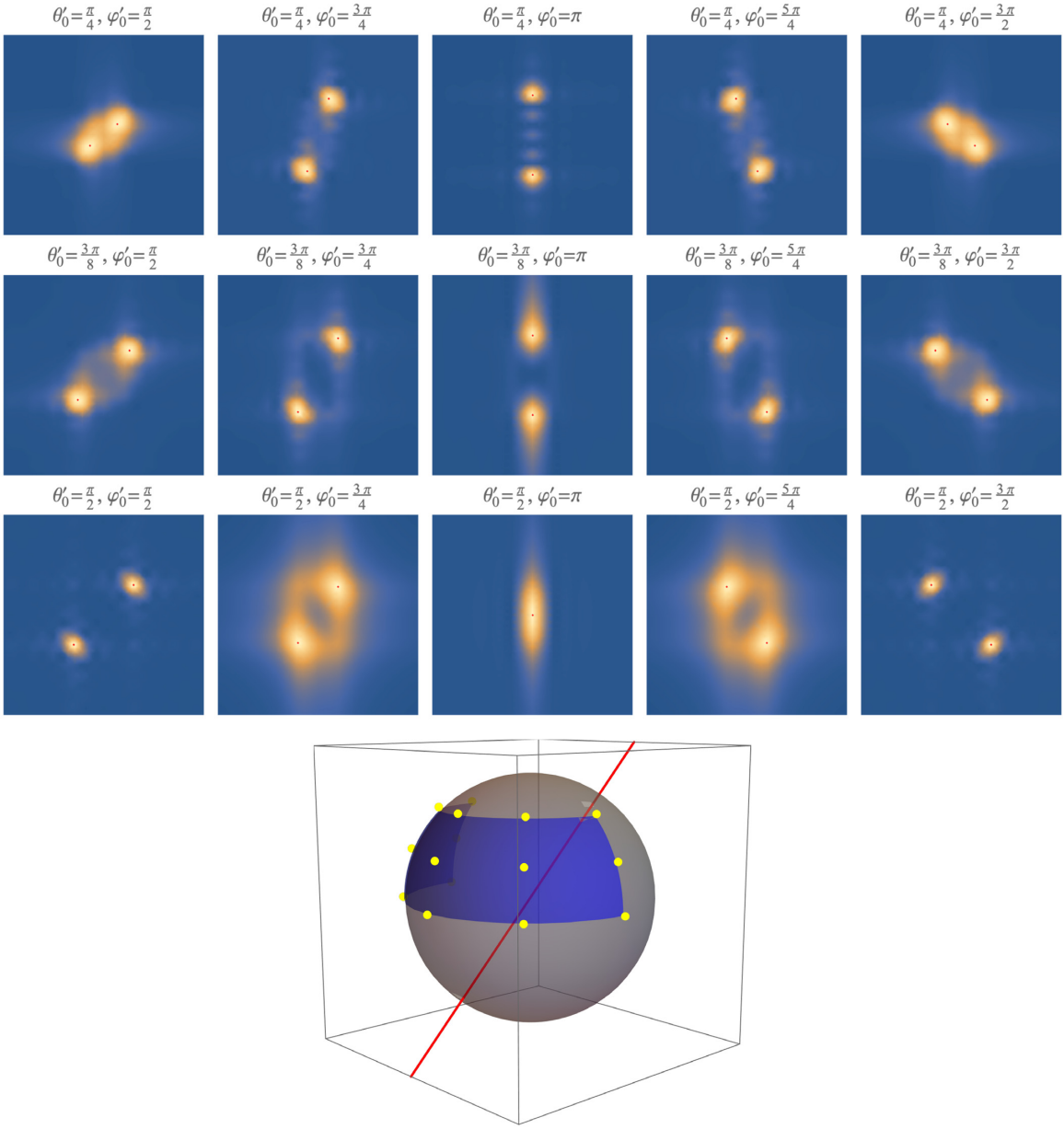


**Fig. 6.** (Top) Images of a fundamental string, with $\theta = \pi/4$. To generate the images from the different relative angles, we have changed $\theta$ instead of the collection of $(\theta', \phi')$, compared to the previous figure. (Bottom) The incoming trajectory (red line) and the observed points on the celestial sphere (yellow circles).

where $c$ is a constant dependent on the choice of $k$ of the central zero, and $f(\theta')$ is some smooth positive function giving the magnitude of the oscillation. This is obvious if we look at the plot of the amplitude in Eq. (29) given in Fig. 7. The amplitude has zeros at Eq. (24) and does not diverge, so it can be approximated by the form in Eq. (30) with a very simple function $f(\theta')$.

The derivation of the explicit form of $f(\theta')$ and the constant $c$ is simple. The latter can be fixed by the distribution of the location of the zeros given in Eq. (24), and the magnitude function $f(\theta')$ can be fixed by evaluating the slope of the amplitude at those zeros. A straightforward

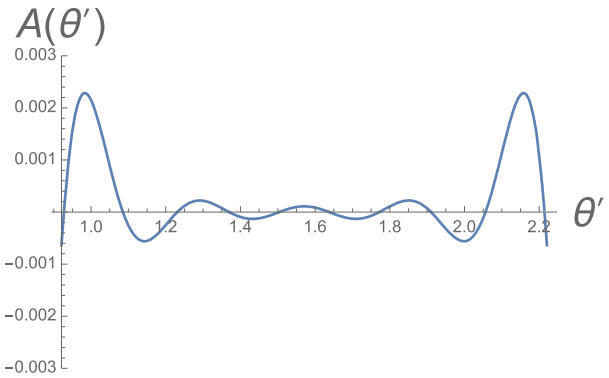


**Fig. 7.** A plot of the amplitude in Eq. (29) for $n = 11$, magnified around $\theta^{'} = \pi/2$.

calculation shows

$$\tilde{\mathcal{A}}_s^{\rm Ven}(\theta') \sim \pm \left[\frac{2}{\pi\ {}_nC_{\frac{n}{2}}}\right] \cos\left(\frac{n\pi}{2}\left(\theta' - \frac{\pi}{2}\right)\right) \qquad (\theta' \sim \theta'_0 = \pi/2) \tag{31}$$

This expression tells us that the magnitude function $f(\theta^{'})$ is constant around $\theta^{'} = \pi/2$. And for a generic $k$ (which means $\theta' \sim \theta'_0$ for generic $\theta'_0$), we find

$$\tilde{\mathcal{A}}_s^{\rm Ven}(\theta') \sim \pm \left[\frac{2}{n\pi\ {}_nC_{\frac{n}{2}(1-\cos\theta'_0)}} \left(\frac{1-\cos\theta'_0}{1+\cos\theta'_0}\right)^{(n\sin\theta'_0/2)(\theta'-\theta'_0)}\right] \cos\left(\frac{n\pi\ \sin\theta'_0}{2}(\theta' - \theta'_0)\right). \tag{32}$$

We can see that the magnitude function $f(\theta^{'})$ is an exponentially growing function. As a consistency check, if one puts $\theta'_0 = \pi/2$ in this expression (32), it reduces to (31).[1]

Let us evaluate the imaging formula in Eq. (28) with these large-$n$ approximated amplitudes in Eqs. (31) and (32). For the case $\theta^{'} \sim \pi/2$, the expression in Eq. (31) is completely the same as that of the double slit in Eq. (3), and we find

$$I_{\theta_0=\pi/2}(X, Y) \propto \sigma(Y)[\sigma(X - \pi p) + \sigma(X + \pi p)] \tag{33}$$

where

$$\sigma(x) \equiv \frac{\sin(pdx)}{pdx}. \tag{34}$$

The function $\sigma$ is, as was described for the case of the double-slit experiment, highly peaked at $x = 0$ in the limit $p \to \infty$. Thus the bright spots in the image are localized at

$$(X, Y) = (\pm\pi p, 0). \tag{35}$$

This is in fact a double slit. In the limit $n \simeq 2p^2 \to \infty$, the image consists of just two bright point-like spots, and the coincidence with the double-slit experiment is exact.

The distance $\Delta$ between the two bright points in the image is given by

$$\Delta = \pi\sqrt{2n} \tag{36}$$

in the string length unit $l_s = 1/\sqrt{2}$ which we took throughout the paper. The behavior $\Delta \sim \sqrt{n}\, l_s$ is consistent with the approximate length of a fundamental string at the excitation level $n$, as we will discuss in Sect. 5.

[1]Note that the difference factor $1/n$ is irrelevant as it comes out by just how the combinatoric factor ${}_nC_{\frac{n}{2}(1-\cos\theta'_0)}$ is evaluated in the sub-leading order in the large $n$ expansion. In any case, the overall constant factor is not the issue in looking at the structure of the images.

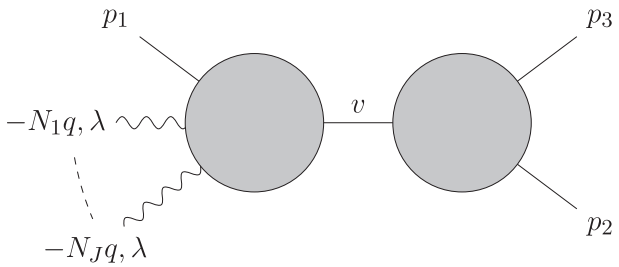


**Fig. 8.** String amplitude of three tachyons and $J$ photons. Picking out a pole at the internal line labeled with $v$ leads to the amplitude of an HES decaying into two tachyons.

Next, let us evaluate the images with the generic $\theta_0'$ using (32). The result is

$$I_{\theta_0=\theta_0'}(X, Y) \propto \sigma\left(\frac{Y}{\sin\theta_0'}\right)\left[\sigma\left(X - \frac{\Delta\left(\theta_0'\right)}{2} + i\tilde{X}_0\right) + \sigma\left(X + \frac{\Delta\left(\theta_0'\right)}{2} + i\tilde{X}_0\right)\right] \tag{37}$$

where

$$\Delta\left(\theta_0'\right) \equiv \pi\sqrt{2n}\sin\theta_0', \quad \tilde{X}_0 \equiv \sqrt{\frac{n}{2}}\left(\sin\theta_0'\right)\log\frac{1+\cos\theta_0'}{1-\cos\theta_0'}. \tag{38}$$

This means that there are two slits which are located, in the complexified coordinates, at

$$(X, Y) = \left(\pm\frac{\Delta\left(\theta_0'\right)}{2} + i\tilde{X}_0, 0\right). \tag{39}$$

The imaginary part contributes to make the peak of $\sigma(x)$ smoother, as the pole deviates from the real axis. The real part gives a physical consistency with the spatial location of the double slit: the distance between the bright spots in the image is $\Delta(\theta_0')$. The factor $\sin\theta_0'$ in this $\Delta(\theta_0')$ is expected from the spatial consistency since the position of the viewer is shifted from the equator and thus the two slits should be seen at an angle, exactly giving the factor $\sin\theta_0'$. Thus we conclude that the images seen at an angle are spatially consistent with each other, which is a nontrivial check for the image slits to be present in the real space.

## 4. Images of HES

In this section, we show that the slit-like behavior of a string is not limited to the Veneziano amplitude. As another clean example, we study an HES decaying to two tachyons.

The amplitude formula for an HES decaying to two tachyons was computed in [5,6]. We will briefly review their results but with slight modifications. Later, we list the location of the amplitude zeros, and point out that these amplitude zeros also match the ones of the double slit in Sect. 2. Then we reconstruct images of an HES by the Fourier transformation of the amplitude. The images show multi-slits, which are understood as convolutions of double slits.

### 4.1. *Amplitude and its zeros*

Following [6], we start with a string scattering amplitude for

$$\text{tachyon, } J \text{ photons} \rightarrow 2 \text{ tachyons}$$

as depicted in Fig. 8. After computing the amplitude, we pick out a pole which corresponds to an intermediate HES state. Momenta of one incoming tachyon and two outgoing tachyons are denoted by $p_1$, $p_2$, and $p_3$. Momenta of $J$ photons are chosen to be proportional to a null vector, $q$, and are given by $-N_a q$, where $N_a$ are integers and $a = 1, \cdots, J$. The momentum conservation

law is

$$0 = (p_1 - Nq) + p_2 + p_3 \tag{40}$$

where

$$N = \sum_{a=1}^{J} N_a, \quad (N_a \geq 1). \tag{41}$$

When a pole of the intermediate state is picked out, $N$ and $J$ will be interpreted as the excitation level and the angular momentum of the HES, respectively. The on-shell conditions for the tachyon momenta are

$$p_1^2 = p_2^2 = p_3^2 = -(-2). \tag{42}$$

For simplicity, polarizations of photons are taken to be equal to each other and denoted by $\lambda$. Then, the conditions for the photon momenta and polarizations are given by

$$q^2 = 0, \quad \lambda^2 = 0, \quad q \cdot \lambda = 0. \tag{43}$$

For simplicity, we assume that

$$(p_2 + p_3) \cdot \lambda = 0. \tag{44}$$

This condition is satisfied, for example, in the center-of-mass frame. Then the amplitude is factorized as

$$\mathcal{A}^{\mathrm{HES}} = \prod_{a=1}^{J} \mathcal{A}_a, \tag{45}$$

$$\mathcal{A}_a = \frac{(-p_2 \cdot \lambda) - (-p_3 \cdot \lambda)}{2} \times \left[ \frac{\Gamma(-\alpha_1^{(a)} + 1)\Gamma(-\alpha_2^{(a)})}{\Gamma(-\alpha_1^{(a)} - \alpha_2^{(a)} + 1)} - \frac{\Gamma(-\alpha_2^{(a)})\Gamma(-\alpha_3^{(a)})}{\Gamma(-\alpha_2^{(a)} - \alpha_3^{(a)})} + \frac{\Gamma(-\alpha_3^{(a)})\Gamma(-\alpha_1^{(a)} + 1)}{\Gamma(-\alpha_3^{(a)} - \alpha_1^{(a)} + 1)} \right], \tag{46}$$

where

$$\alpha_i^{(a)} = N_a p_i \cdot q. \tag{47}$$

Each factor of the amplitude, $\mathcal{A}_a$, has poles when $1 - \alpha_1^{(a)}$ is a negative integer. Poles at

$$\alpha_1^{(a)} \sim N_a \tag{48}$$

are located at the same position in the momentum space,

$$v = -(p_1 - Nq)^2 \sim 2(N - 1). \tag{49}$$

Picking out this pole, we have an HES at an intermediate state. By taking the residues of $\mathcal{A}_a$, we obtain the decay of the HES with the mass

$$M^2 = 2(N - 1), \tag{50}$$

and the total angular momentum $J$. Using an identity $\alpha_1^{(a)} + \alpha_2^{(a)} + \alpha_3^{(a)} = 0$, and the condition of the pole, $\alpha_1^{(a)} \sim N_a$, we find

$$\begin{aligned}\tilde{\mathcal{A}}_v^{\rm HES} &= \lim_{v\to 2(N-1)} \left(\prod_{a=1}^{J} \frac{\sin\pi\alpha_1^{(a)}}{\pi}\right) \mathcal{A}^{\rm HES} \\ &= \prod_{a=1}^{J} \frac{(-p_2\cdot\lambda)-(-p_3\cdot\lambda)}{2} \left[\frac{\Gamma(-\alpha_2^{(a)})}{\Gamma(N_a)\Gamma(-\alpha_2^{(a)}-N_a+1)} + (2\leftrightarrow 3)\right] \\ &= \prod_{a=1}^{J} \frac{(-p_2\cdot\lambda)-(-p_3\cdot\lambda)}{2} \left[\frac{\Gamma(-\alpha_2^{(a)})}{\Gamma(N_a)\Gamma(\alpha_3^{(a)}+1)} + (2\leftrightarrow 3)\right]. \end{aligned} \tag{51}$$

Here, the first term is a contribution studied in [6].

In the center-of-mass frame, we take the following parametrization of the momenta,

$$-q = \frac{1}{\sqrt{2N-2}}\begin{pmatrix}1\\0\\0\\-1\end{pmatrix}, \quad \lambda = \frac{1}{\sqrt{2}}\begin{pmatrix}0\\1\\i\\0\end{pmatrix}, \tag{52}$$

$$p_1 - Nq = \begin{pmatrix}\sqrt{2N-2}\\0\\0\end{pmatrix}, \quad -p_2 = \begin{pmatrix}\sqrt{2N-2}/2\\ \sqrt{2N+6}/2\ \sin\theta'\\0\\ \sqrt{2N+6}/2\ \cos\theta'\end{pmatrix}, \quad -p_3 = \begin{pmatrix}\sqrt{2N-2}/2\\ -\sqrt{2N+6}/2\ \sin\theta'\\0\\ -\sqrt{2N+6}/2\ \cos\theta'\end{pmatrix}. \tag{53}$$

Under this parametrization, the variables $\alpha_i^{(a)}$ are expressed as

$$\alpha_1^{(a)} = N_a, \tag{54}$$

$$\alpha_2^{(a)} = -\frac{N_a}{2}\left(1 + \frac{\sqrt{2N+6}}{\sqrt{2N-2}}\cos\theta'\right), \tag{55}$$

$$\alpha_3^{(a)} = -\frac{N_a}{2}\left(1 - \frac{\sqrt{2N+6}}{\sqrt{2N-2}}\cos\theta'\right). \tag{56}$$

Let us look for zeros of the amplitude in Eq. (51). It is zero if and only if

$$0 = (-p_2\cdot\lambda) = -(-p_3\cdot\lambda), \tag{57}$$

$$\text{or} \qquad 0 = \Gamma\left(-\alpha_2^{(a)}\right)\Gamma\left(\alpha_2^{(a)}+1\right) + (2\leftrightarrow 3) \tag{58}$$

for some $1 \le a \le J$. Calculations similar to those in Sect. 3 show that the amplitude is trivially zero if some $N_a$ is even. In the following discussion, we assume that $N_a$'s are odd for any $1 \le a \le J$. Then we find that the zeros of the amplitude are at

$$\frac{\sqrt{2N+6}}{\sqrt{2N-2}}\cos\theta' = \frac{2\mathbf{Z}-1}{N_a}. \tag{59}$$

In the high excitation limit $N_a \to \infty$, it is written as

$$\cos\theta' \simeq \frac{k'}{N_a}, \tag{60}$$

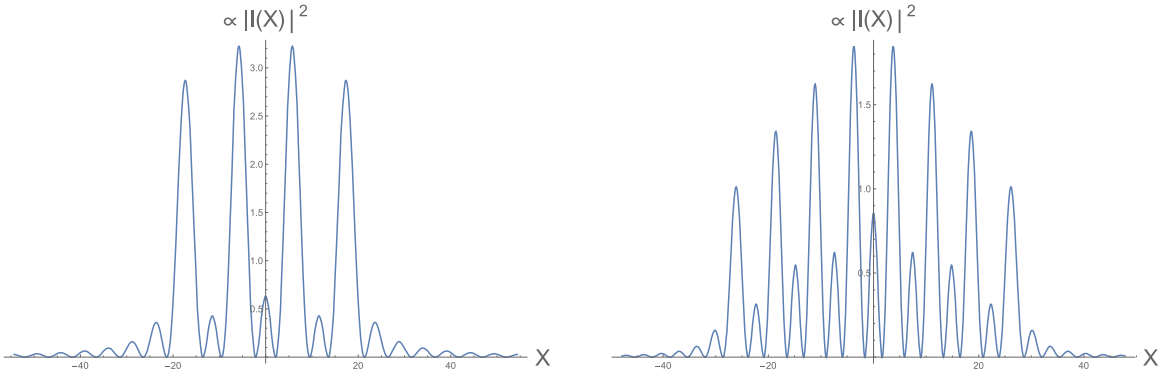


**Fig. 9.** Images of an HES, extracted and reconstructed from an HES intermediate-state pole of the tachyon–photon amplitude. The size of the imaging lens is chosen as $d = 0.11$. The left panel, for a division $N = N_1 + N_2 = 19 + 39$, shows a 4-slit, while the right panel, for $N = N_1 + N_2 + N_3 = 19 + 39 + 79$, shows an 8-slit.

where $k'$ is an odd integer, $k' \in 2\mathbf{Z} - 1$. We find that the location of the zeros is exactly the same as that of the double-slit experiment, Eq. (2), with the replacement

$$\frac{N_a}{2} = \frac{l}{\lambda_{\rm ds}}. \tag{61}$$

Here $N_a$ is an excitation level of the $a$-th mode such that $N = \sum_a N_a$, while $l$ ($\lambda_{\rm ds}$) is the slit separation (wavelength) in the double-slit experiment.

### 4.2. *Imaging of an HES*

Here first we present images of an HES by straightforward numerical evaluations, and then understand the images analytically in a certain limit.

Since the amplitude depends only on the outgoing angle $\theta'$, we restrict ourselves to imaging in this single direction. We use the following imaging formula:

$$I(X) = \frac{1}{(2d)^2 \sin\theta_0'} \int_{\theta_0'-d}^{\theta_0'+d} d\theta' e^{ip(\theta'-\theta_0')X} \tilde{\mathcal{A}}_v^{\rm HES}(\theta'). \tag{62}$$

Here $p$ is now the magnitude of the outgoing tachyon momentum $p = \sqrt{2N+6}/2$. A straightforward numerical evaluation of the imaging formula Eq. (62) produces the images shown in Fig. 9. Both of the images are for $\theta_0' = \pi/2$, but with different numbers of excitations of $N = \sum_{a=1}^{J} N_a$. We find that the images of an HES are those of multi-slits.

Such multi-slit structures can simply be understood by using the results in the Veneziano amplitude. When $N_a \gg 1$, the amplitude in Eq. (51) reduces to a simple form:

$$\tilde{A}_v^{\rm HES} \simeq \prod_{a=1}^{J} \sin\theta' \left[ \frac{\Gamma\left(+\frac{N_a}{2}(1+\cos\theta')\right)}{\Gamma\left(-\frac{N_a}{2}(1-\cos\theta')\right)} + \frac{\Gamma\left(+\frac{N_a}{2}(1-\cos\theta')\right)}{\Gamma\left(-\frac{N_a}{2}(1+\cos\theta')\right)} \right] \tag{63}$$

up to a constant. Remark that each factor inside $\prod_{a=1}^{J}$ coincides with the Veneziano amplitude at $\theta = 0$ (29) with the replacement $n \to N_a$,

$$\tilde{\mathcal{A}}_v^{\rm HES} \simeq (\sin\theta')^J \prod_{a=1}^{J} \tilde{\mathcal{A}}_s^{\rm Ven}\Big|_{n\to N_a}. \tag{64}$$

Thus the reconstructed image of an HES, the Fourier transformation of $\tilde{\mathcal{A}}_v^{\rm HES}$, is the convolution of the images of the Veneziano amplitudes with $n \to N_a$ as,

$$I^{\rm HES} \simeq (\sin\theta')^J * I^{\rm Ven}\big|_{n\to N_1} * \cdots * I^{\rm Ven}\big|_{n\to N_J} . \tag{65}$$

Recall that the image of the Veneziano amplitude $I^{\rm Ven}$ is a double slit with a slit separation $l/\lambda_{\rm ds} \simeq n/2$. With replacements $n \to N_a$, $\lambda_{\rm ds} \to 1/\sqrt{N}$, the image of an HES is the convolution of double slits with separations $\Delta_a \sim N_a/\sqrt{N}$. Then we can conclude that the image of an HES is a $2^J$-slit. Indeed it can be easily demonstrated that the convolution of double slits with different slit separations is a multi-slit. Let

$$I_a(X) = \delta\left(X - \frac{\Delta_a}{2}\right) + \delta\left(X + \frac{\Delta_a}{2}\right) \tag{66}$$

be an ideal image of a double slit with the slit separation $\Delta_a$. Then its convolution

$$\begin{aligned} I_a * I_b(X) &= \int_{-\infty}^{\infty} {\rm d}X'\ I_a(X') I_b(X - X') \\ &= \sum_{s_1,s_2=\pm 1} \delta\left(X + s_1\frac{\Delta_a}{2} + s_2\frac{\Delta_b}{2}\right) \end{aligned} \tag{67}$$

is a $2^2$-slit. Performing similar operations recursively, we can show that $J$-times convolution of the double slit with different slit-separations is a $2^J$-slit as:[2]

$$I_1 * \cdots * I_J(X) = \sum_{s_a=\pm 1} \delta\left(X + s_1\Delta_1 \cdots + s_J\Delta_J\right). \tag{68}$$

We conclude that the image of the HES reconstructed from its decay amplitude is a multi-slit.

## 5. Interpretation

In this section, we present several observations from the results obtained above, and provide their possible interpretations.

Firstly, we point out that the slit-like appearance of scattering amplitude images is an inherent feature of strings. Recall, for example, the Veneziano amplitude. At the zeros of the amplitude in Eq. (24), each term of Eq. (16) becomes zero simultaneously. There is no nontrivial cancellation between the two terms. In other words, the zeros of the amplitude originate in the gamma functions in the denominator. These gamma functions are also the source of poles which correspond to intermediate excited string states. Thus the existence of a series of zeros in Eq. (24) reflects the existence of a series of intermediate states in string theory. Remember that, contrary to string theory, perturbative quantum field theories have only a few intermediate states, and scatterings occur at a point.

Secondly, it is remarkable that the order of slit separations agrees with that of the total string length. Recall that the slit separations in the Veneziano amplitude and in the HES scattering amplitude (with $J = 1$) are

$$\Delta^{\rm Ven} \sim \sqrt{n}\, l_s, \quad \Delta^{\rm HES} \sim \sqrt{N}\, l_s, \tag{69}$$

respectively. Here $n$ is roughly the square of the invariant mass, and $N$ is roughly the square of the mass of an HES. On the other hand, the total length of a string with a mass $M$ is roughly estimated as

$$l_{\rm total} \sim \frac{1}{\alpha'} M \sim \sqrt{N}\, l_s \tag{70}$$

[2]Particularly when $\Delta_a/\Delta_1 \simeq 2^a$, the slits are equally separated.

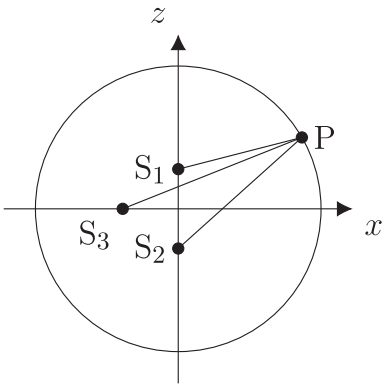


**Fig. 10.** Three slits are put at $S_1$, $S_2$, $S_3$, and the scattered wave is observed at point P.

since a string has a constant tension $\alpha'$. Thus, the slit separation and string length coincide with each other, meaning that the string may extend between the slits.

Thirdly, we stress that slits can only show up on a straight line both in the Veneziano amplitude and in the HES amplitude. Technically, this is because the $\theta'$ dependence of their amplitude zeros is only in the form of $\pm\cos\theta'$. In fact, other types of $\theta'$ dependence with nontrivial phases $\cos(\theta' - \vartheta')$ are required for the slit to show up away from the straight line. This can be easily demonstrated as follows. Suppose that we have three slits $S_1$, $S_2$, $S_3$ which are not on a straight line as in Fig. 10. If the location of $S_3$ is $(z, x) = (0, -l'/2)$, the optical path lengths are

$$\overline{S_1P} - \overline{OP} = -\frac{l}{2}\cos\theta', \tag{71}$$

$$\overline{S_2P} - \overline{OP} = +\frac{l}{2}\cos\theta', \tag{72}$$

$$\overline{S_3P} - \overline{OP} = +\frac{l'}{2}\cos(\theta' - \pi/2). \tag{73}$$

Thus the location of the amplitude zeros depends not only on $\pm\cos\theta'$ but also on the phase-shifted $+\cos(\theta' - \pi/2)$.[3]

From these observations, we can provide an interpretation that the locations of slits are the end points of a string. Firstly, we should remark that the order of the slit separation is not the random walk size $l \sim M^{1/2} \sim N^{1/4}$, but rather it is the total length of the string $L \sim M \sim N^{1/2}$. It motivates us to assume that the string behaves like a simple harmonic oscillator in the scattering processes.

Then there remain two possibilities: the locations of slits indicate (i) the nodes, or (ii) the end points, of the vibrating string. The first possibility is excluded since the HES amplitude with $J = 1$, $N \gg 1$ behaves like a double slit as discussed in Sect. 4. If the nodes of the vibrating string are the origin of the slit image, the HES image with $J = 1$, $N \gg 1$ would have been a multi-slit, rather than the double slit. Since this is not the case, thus we are left with possibility (ii): slits are end points of the string.

Such an interpretation is also supported by the following scenarios. Suppose there is a classical vibrating string with markers attached to its end points, as an analogy of the world sheet with open string vertex operators inserted at its boundary. The long time average of the

[3]The existence of such a slit-like structure within a scattering region is a sign of chaos. The chaoticity of string scatterings will be discussed in the authors' next paper [10].

probability that the markers are found at a point $X$ is roughly evaluated by

$$\int_0^T \frac{\mathrm{d}t}{T}\,\delta(X - X_0 \sin\omega t) \sim \frac{1}{\sqrt{X_0^2 - X^2}}. \tag{74}$$

Then it becomes maximum at the point where the string is fully extended to its maximum size. This is consistent with our results where slits are separated at a distance of the order of the total string length.

Another scenario is about the origin of interference patterns. Suppose that two incoming strings are shot along the $z$-direction and scattered at the origin. Our results have shown that if this scattering is observed from the $x$-direction, the image is the double slit lined up along the $z$-direction. It would be natural to imagine that a string formed at the origin vibrates along the $z$-direction, and is torn apart when the string reaches its maximum length. Each of the two pieces of the broken string can be scattered in any directions, though one must go in the opposite direction to the other. The observer in the $x$-direction can detect the scattered string with a definite probability. At the observation, the observer has two possibilities: the left one of the two pieces of the broken string reaches the observer while the right one goes in the opposite direction, or vice versa. The superposition of these two possibilities would be the source of the interference patterns which appear in the string scattering amplitudes.

These scenarios encourage us to state that the slits are the end points of a fundamental string.

**Acknowledgements**

The work of K.H. was supported in part by Japan Society for the Promotion of Science (JSPS) KAKENHI Grant Nos. JP22H01217, JP22H05111, and JP22H05115. The work of Y.M. was supported in part by JSPS KAKENHI Grant Nos. JP20K03930, JP21H05182, and JP21H05186. The work of T.Y. was supported in part by JSPS KAKENHI Grant No. JP22J15276. The work of K.H. and Y.M. was also supported in part by JSPS KAKENHI Grant No. JP17H06462. K.H. would like to thank Yannick Paget for discussions and collaborative artwork concerning this research.

## Funding

Open Access funding: SCOAP[3].

## References

[1] G. T. Horowitz and J. Polchinski, Phys. Rev. D **55**, 6189 (1997). [hep-th/9612146].
[2] G. T. Horowitz and J. Polchinski, Phys. Rev. D **57**, 2557 (1998). [hep-th/9707170].
[3] E. Halyo, B. Kol, A. Rajaraman, and L. Susskind, Phys. Lett. B **401**, 15 (1997). [hep-th/9609075].
[4] L. Susskind, [arXiv:2110.12617] [Search inSPIRE].
[5] D. J. Gross and V. Rosenhaus, JHEP **05**, 048 (2021), [arXiv:2103.15301] [Search inSPIRE].
[6] V. Rosenhaus, Phys. Rev. Lett. **129**, 031601 (2022), [arXiv:2112.10269] [Search inSPIRE].
[7] K. Hashimoto, S. Kinoshita, and K. Murata, Phys. Rev. D **101**, 066018 (2020), [arXiv:1811.12617] [Search inSPIRE].
[8] K. Hashimoto, S. Kinoshita, and K. Murata, Phys. Rev. Lett. **123**, 031602 (2019) [arXiv:1906.09113] [Search inSPIRE].
[9] G. Veneziano, Nuovo Cim. A **57**, 190 (1968).
[10] K. Hashimoto, Y. Matsuo, and T. Yoda, JHEP **11**, 147 (2022) [arXiv:2208.08380].